Visual Field Maps, Population Receptive Field Sizes, and Visual Field Coverage in the Human MT+ Complex

Kaoru Amano,[1,2] **Brian A. Wandell,**[1] **and Serge O. Dumoulin**[1,3]

[1]*Department of Psychology, Stanford University, Stanford, California;* [2]*Graduate School of Frontier Sciences, The University of Tokyo, Chiba, Japan; and* [3]*Helmholtz Institute, Experimental Psychology Division, Utrecht University, Utrecht, The Netherlands*

Amano K, Wandell BA, Dumoulin SO. Visual field maps, population receptive field sizes, and visual field coverage in the human MT+ complex. *J Neurophysiol* 102: 2704–2718, 2009. First published July 8, 2009; doi:10.1152/jn.00102.2009. Human neuroimaging experiments typically localize motion-selective cortex (MT+) by contrasting responses to stationary and moving stimuli. It has long been suspected that MT+, located on the lateral surface at the temporal–occipital (TO) boundary, contains several distinct visual field maps, although only one coarse map has been measured. Using a novel functional MRI model–based method we identified two maps—TO-1 and TO-2—and measured population receptive field (pRF) sizes within these maps. The angular representation of the first map, TO-1, has a lower vertical meridian on its posterior side at the boundary with the lateral–occipital cortex (i.e., the LO-2 portion). The angular representation continues through horizontal to the upper vertical meridian at the boundary with the second map, TO-2. The TO-2 angle map reverses from upper to lower visual field at increasingly anterior positions. The TO maps share a parallel eccentricity map in which center-to-periphery is represented in the ventral-to-dorsal direction; both maps have an expanded foveal representation. There is a progressive increase in the pRF size from V1/2/3 to LO-1/2 and TO-1/2, with the largest pRF sizes in TO-2. Further, within each map the pRF size increases as a function of eccentricity. The visual field coverage of both maps extends into the ipsilateral visual field, with larger sensitivity to peripheral ipsilateral stimuli in TO-2 than that in TO-1. The TO maps provide a functional segmentation of human motion-sensitive cortex that enables a more complete characterization of processing in human motion-selective cortex.

INTRODUCTION

Neuroimaging experiments localize human motion-selective cortex by contrasting the responses to moving and stationary stimuli (Tootell et al. 1995; Watson et al. 1993; Zeki et al. 1991). Many locations within visual cortex respond differentially to moving and static stimuli, but the most powerful responses are found in the posterior part of the inferior temporal sulcus (Dumoulin et al. 2000). This region contains the human homologue of middle temporal area (MT) but also parts of several surrounding motion-selective areas, such as dorsal/lateral medial superior temporal area (MSTd/MSTl) and fundus of the superior temporal sulcus (FST), known to exist in nonhuman primates. DeYoe et al. (1996) coined the term "MT+" pending clarification by additional experiments.

Defining human MT+ based on stimulus selectivity means that the identification of the region borders depends on factors such as the response–amplitude threshold and the instrumental signal-to-noise ratio. It is desirable to create methods for identifying motion-selective cortex based on more objective criteria such as retinotopy. This should be possible because the first description of MT in owl monkey was based on its retinotopic organization (Allman and Kaas 1971). In human, however, MT+ retinotopy using conventional traveling wave methods with rings and wedges has shown only one coarse visual field eccentricity map, which is proposed to be a homologue of monkey MT (Huk et al. 2002).

Here we use a new method of retinotopic mapping (Dumoulin and Wandell 2008) to reveal retinotopic representations and population receptive field (pRF) sizes in MT+. The method is especially suitable for mapping motion-sensitive regions, which contain large receptive field sizes that span the vertical midline (Dumoulin and Wandell 2008). We find that MT+ contains at least two hemifield representations. We label these maps by their location in the temporal–occipital cortex (TO-1 and TO-2). We use this naming convention because there is uncertainty about homology with monkey maps and the relationship between these maps and those described in a previous study (Huk et al. 2002). It is likely, however, that TO-1/TO-2 correspond to MT and MSTl in macaque. We show that these maps form part of a continuous series of maps originating in V1, which enables the definition of motion-sensitive visual field maps based on retinotopy, rather than localizer experiments.

METHODS

Subjects

Seven subjects participated in this study. All subjects had normal or corrected-to-normal visual acuity. Informed written consent was obtained from all subjects. All subjects participated in scanning sessions to obtain not only a T1-weighted anatomical volume but also functional sessions to measure the visual field maps and responses to MT/MST (Huk et al. 2002) and lateral–occipital complex (LOC) localizer stimuli (Grill-Spector and Malach 2004; Malach et al. 1995).

Stimulus presentation

Visual stimuli were generated using the Psychophysics Toolbox (Brainard 1997; Pelli 1997) in the Matlab programming environment on a Macintosh G4 Powerbook. The display configuration consisted of a liquid crystal display projector (NEC LT158), with optics that imaged the stimuli onto a back-projection screen in the bore of the magnet. The stimulus radius was 10° (five subjects) or 14° (two subjects) of visual angle. The subjects viewed the display through a mirror.

Address for reprint requests and other correspondence: K. Amano, Biological Complex Systems Laboratory, Department of Complexity Science and Engineering, Graduate School of Frontier Sciences, The University of Tokyo, 5-1-5, Kashiwanoha, Kashiwa-shi, Chiba 277-8561, Japan (E-mail: amano@brain.k.u-tokyo.ac.jp).

During stimulus presentation, the subjects fixated on a small (~0.5°) fixation disc. They were instructed to press a button every time the fixation disc changed color. The response accuracies were >90%.

Visual field mapping and pRF stimuli

The stimuli included wedge, ring, and bar apertures that exposed moving contrast patterns. At regular intervals the apertures were removed and the subject saw only the zero-contrast (mean-luminance) background. These stimuli are effective at revealing visual field maps with large receptive fields like MT+ (Dumoulin and Wandell 2008). The aperture positions were displaced in discrete steps in synchrony with the functional magnetic resonance imaging (fMRI) volume acquisition, i.e., every 3 s. The wedge aperture subtended 45° and widths of the rings and bar apertures were one third of the stimulus radius. The contrast patterns exposed by the wedge and ring apertures comprised a moving dartboard. Each spoke of the dartboard (15° angle) moved in opposite directions. The bar aperture revealed a checkerboard contrast pattern and adjacent rows of the exposed checkerboard moved in opposite directions along the longest axis of the bar. The contrast pattern motion created a 2-Hz temporal frequency; the motion direction changed randomly (about every 2–3 s). A full cycle of wedge and ring stimuli was 36 s, with a total of six cycles (216 s) per scanning run. Four bar orientations (0, 45, 90, and 135° from vertical) and two different motion directions orthogonal to each bar orientation were used, giving a total of eight different bar configurations within a given scan for 240 s. Three to five scans (wedge/ring) and five to seven scans (bar) were performed for each subject in one or two sessions.

Four mean-luminance periods were inserted during the last 18 s of every 54 s (wedge/ring) or during the last 12 s of every 60 s (bar). It should be noted that the rate of the mean luminance periods (4 cycles/scan) differs from the stimulus period (six cycles/scan for wedge/ring and one cycle/scan for bar). Thus each mean-luminance presentation replaces a different position of the wedge, ring, or bar stimulus. The mean-luminance periods are necessary for accurate estimation of large pRF sizes (Figs. 1 and 3 of Dumoulin and Wandell 2008).

Visual field mapping and pRF analysis

We used a model-based method to estimate visual field maps and population receptive fields (pRFs) (Dumoulin and Wandell 2008). The pRF is defined as the region of visual space that stimulates the recording site (Dumoulin and Wandell 2008; Jancke et al. 2004; Victor et al. 1994). Briefly, for each voxel we predicted the blood oxygen level–dependent (BOLD) response using a two-dimensional (2D) Gaussian pRF model; the parameters are center location (x, y) and spread (σ). The predicted fMRI time series is calculated by a convolution of the model pRF with the stimulus sequence and the BOLD hemodynamic response function (HRF) (Boynton et al. 1996; Friston et al. 1998; Glover 1999b; Worsley et al. 2002); the pRF parameters for each voxel minimize the sum of squared errors between the predicted and observed fMRI time series for all stimuli (wedges, rings, and bars). Further details of the pRF analysis are described in a previous study (Dumoulin and Wandell 2008).

Angle $\tan^{-1}(y/x)$, eccentricity $\sqrt{(x^2 + y^2)}$, and pRF size (σ) maps are derived from the fitted 2D Gaussian models. These parameters are shown on the unfolded cortical surface measured in each subject (Figs. 1, 2, 5B, and Supplemental Figs. S1–S8).[1] We show parameter map estimates only when the response coherence exceeds 0.32. Using the complementary error function (Bandettini et al. 1993), this coherence threshold corresponds to $P \ll 0.001$ uncorrected and $P < 0.01$ Bonferroni corrected for multiple comparisons within the volume of

scanned cortex. However, because we select the best fit from a large range of possible predictions we also computed the null distribution empirically (Grill-Spector et al. 2006). Using this method, the coherence threshold (0.32) corresponds to $P < 0.05$. Flattened representations were derived using the methods described in Wandell et al. (2000).

Visual field coverage

Visual field coverage defines the locations within the visual field that evoke a significant response from voxels within a map. We estimate the visual field coverage from the full pRF. We first identify the pRF centers across all of the voxels within a visual field map. For each subject, we create a binary image showing whether a pRF center exists at each visual field location. The binary images of the centers are pooled across subjects to obtain the averaged pRF center plots (Fig. 7, *left panels*). We estimate the visual field coverage by combining the pRF center and size estimates. Specifically, from each voxel we estimate the 2D Gaussian in the visual field (stimulus-referred). Many points in the visual field are covered by at least one pRF and we create a map that represents the highest pRF value at each visual field location. Because the peak value of the 2D Gaussian model is normalized to 1, the range of values in each subject's map is between 0 and 1. We create these maps for each subject, and then average the maps from all subjects. For example, if a particular location in the visual field is at the center of a pRF in all 14 hemispheres, the average map contains a 1 at that location. Conversely, if no pRF covers that visual field location the value is zero. Thus the visual field coverage levels range from 0 to 1, as well.

To represent a single pRF centers or visual field coverage map combining all hemispheres, we convert the right hemisphere data into left-hemisphere format.

Motion localizer stimuli

The locations of MT+ (Tootell et al. 1995; Watson et al. 1993; Zeki et al. 1991) and tentative MST (Huk et al. 2002) were identified from the functional responses to stimuli that alternated between moving and stationary dot patterns. The MT+ and MST localizers used here are the same as those used by Huk et al. (2002). In the MT+ localizer there is a 9-s motion block and a 27-s stationary block. During the motion block white dots on a black background were presented within a 10° diameter circular aperture, centered at the fixation. The dots (0.25° in width) moved coherently toward and away from fixation at 8°/s, alternating direction once per second. Each dot appeared for 167 ms (10 frames) and was then replaced by another dot at a randomly selected position. Two hundred dots were used within the aperture. The moving/stationary pair was repeated six times in each fMRI scan (scan duration of 3.6 min). This MT+ localizer scan was repeated three to six times for each subject.

The MST localizer alternated between 18-s peripheral moving dots and 18-s static dots. In this case 200 moving and stationary dots were presented within a peripheral ipsilateral circular aperture (15° in diameter) with its closest edge 10° from fixation. This moving/stationary cycle was repeated 6 times in each fMRI scan; the MST localizer scan was repeated 5–11 times in each hemifield for each subject. The additional MST localizer scans are necessary because the response to these dots in the ipsilateral periphery is much weaker than the response when the dots are presented in central vision (Huk et al. 2002). The MT+ and MST localizer scans were performed in one or two sessions.

LOC localizer stimuli

The position of the LOC was determined from the functional responses to objects and faces. In one type of block (O) subjects saw grayscale images of cars and sculptures; in a second type of block

---

[1] The online version of this article contains supplemental data.

subjects saw faces (F). In a third block subjects saw scrambled versions of these images (S); the images were scrambled by dividing them into an 8 × 8 grid of tiles and then randomly reassigning the tile positions. Images were presented within a central 10° radius aperture. Object/scrambled (OS) and face/scrambled (FS) cycles (12-s O/F and 12-s S) were repeated in each scan, according to the three repetitions of the sequence OSFSFSOS (scan duration of 4.8 min). Five to six LOC localizer scans were performed in one session.

Anatomical data

T1-weighted anatomical images were acquired on a 1.5-T Sigma LX scanner with a vendor-supplied head-coil using a three-dimensional (3D)–SPGR (i.e., spoiled gradient recalled acquisition in steady state) pulse sequence (one echo, minimum echo time [TE], flip angle: 15°, effective voxel size: $0.94 \times 0.94 \times 1.2$ mm³). We acquired at least two whole brain T1-weighted anatomical MRI data sets for each subject. These data were averaged and resampled to a 1-mm³ isotropic resolution. The surface-coil anatomical MRI, taken at the same time as the functional images, was aligned with the head-coil anatomical MRI using a mutual information method (Ashburner and Friston 2003; Maes et al. 1997). The functional images and surface-coil anatomical data acquired in the same session were coregistered. Using the spiral acquisition and small field-of-view (FOV) surface-coil limits the spatial distortions between the functional and surface-coil anatomical images. Thus we used the transformation derived from the surface-coil anatomicals to align the functional data to the head-coil anatomicals.

White matter was segmented from the head-coil anatomical MRI using custom software and hand-edited to minimize segmentation errors (Teo et al. 1997). Gray matter was grown from the segmented white matter to form a 2- to 4-mm layer covering the white-matter surface. The cortical surface was represented as a mesh at the white/gray-matter border. This mesh was used to render a smoothed 3D cortical surface or to flatten the cortical representation (Wandell et al. 2000). In the smoothed 3D representations dark regions indicate sulci and light regions indicate gyri.

Functional data

Functional magnetic resonance images were acquired with a 3-T General Electric Sigma scanner and an eight-channel surface coil (Nova Medical, Wilmington, MA) centered over the subject's occipital pole. The effective voxel size was 1.5 mm isotropic (FOV = 19.2×19.2 cm²). Functional MR images (repetition time/TE: 3,000/30 ms, flip angle: 71°) were acquired using a self-navigated spiral-trajectory pulse sequence (Glover 1999a; Glover and Lai 1998) with 20 axial slices covering lateral–occipital and temporal–occipital cortices with no gap.

We analyzed fMRI data using custom software (http://vistalab. stanford.edu/software/). Data in each fMRI session were analyzed voxel by voxel with no spatial smoothing. The acquired BOLD signal from each voxel was transformed to a percentage modulation about the mean. Baseline drifts were deducted from the time series by high-pass temporal filtering. Head movements across scans were examined by comparing the mean value maps of the BOLD signals and a motion-correction algorithm was applied; most scans had minimal head motion (less than one voxel). Motion artifacts within each scan were also monitored, but the within-scan motion was not corrected because it was always very small. Fewer than 10% of the scans had significant motion artifacts; these scans were discarded.

Atlas fitting

The visual field map borders were identified by fitting a quantitative model of the expected map (the atlas) to the measured data (Dougherty et al. 2003). This atlas-fitting procedure was performed separately for the group of LO-1/2 and TO-1/2 maps and the group of V1/V2/V3 maps.

The LO-1/2, TO-1/2 atlas included four hemifields whose angle maps changed from lower to upper (LO-1), upper to lower (LO-2), lower to upper (TO-1), and upper to lower (TO-2) vertical meridian. The atlas for V1/V2/V3 included two upper quadrants (V3v, V2v), one hemifield (V1), and two lower quadrants (V2d, V3d). The atlases contained orthogonal eccentricity and angle maps.

In the atlas-fitting procedure a template of the expected angle and eccentricity maps (1–10°) is aligned to the individual maps by hand. In this alignment, the user defines a quadrilateral that defines the four sides of the visual field map, from fovea to periphery and from upper to lower vertical meridian, by simultaneously looking at angle and eccentricity maps to visually detect the point of angle reversal at the eccentricity of 1 and 10°. The fitting algorithm deforms these templates to match the eccentricity and angle data, allowing local deformations but no tears or folds in the atlas. The least-squares error between the atlas and the data are determined at all locations covered by the initial placement of the atlas and weighted by the coherence of the data. The algorithm simultaneously fits the angle and eccentricity maps (Dougherty et al. 2003; Heyder 2006). The boundaries identified by atlas fitting correspond well to those drawn by manual inspection, and the area estimates obtained by the two methods were very similar.

Atlas-based averaging

To increase the power of our analysis, we average the visual field maps from all subjects onto an average flattened representation. We first find atlas fits to individual subject maps using the procedure defined earlier. During this procedure, the user initiates the process by defining a quadrilateral that defines the four sides of the visual field map. The fitting algorithm returns a deformation between this quadrilateral and the data on the user's flattened representation. We apply the inverse of the atlas deformation to the individual's raw data, transforming the data into the initial quadrilateral position. Then, we combine the data across observers by finding the affine transformation that converts the four corners of each quadrilateral into a common reference frame (Larsson and Heeger 2006). This transforms the data from individual flat maps into a single common reference frame. The average maps (Fig. 3, 6B, and Fig. 8, B, D, and F) are generated by averaging the angle, eccentricity, and pRF size data from each subject in this common reference frame. Individual subject data are weighted by response coherence.

RESULTS

Visual field maps TO-1 and TO-2

Figures 1 and 2 contain angle maps and eccentricity maps. The data in Fig. 1 are from one particularly clear subject (S2), whereas the data in Fig. 2 are from six hemispheres that illustrate the variability across subjects. The *inset* in Fig. 1 shows the MT+ localizer responses. The maps of all 14 hemispheres are shown in Supplemental Figs. S1, S2, S5, and S6.

We model the data in this region as comprising four maps anterior to V3d, each representing a hemifield. The first two maps correspond to LO-1 and LO-2 (Larsson and Heeger 2006), which are known to overlap with the posterior part of the object-selective LOC. We can confidently localize the two most anterior maps as falling within MT+ because of *1*) their anatomical location (Dumoulin et al. 2000) and *2*) the correspondence with a conventional motion localizer (shown in Fig. 1, *inset* and Fig. 8). Because of uncertainty about homology with monkey areas, and to emphasize the retinotopic definition
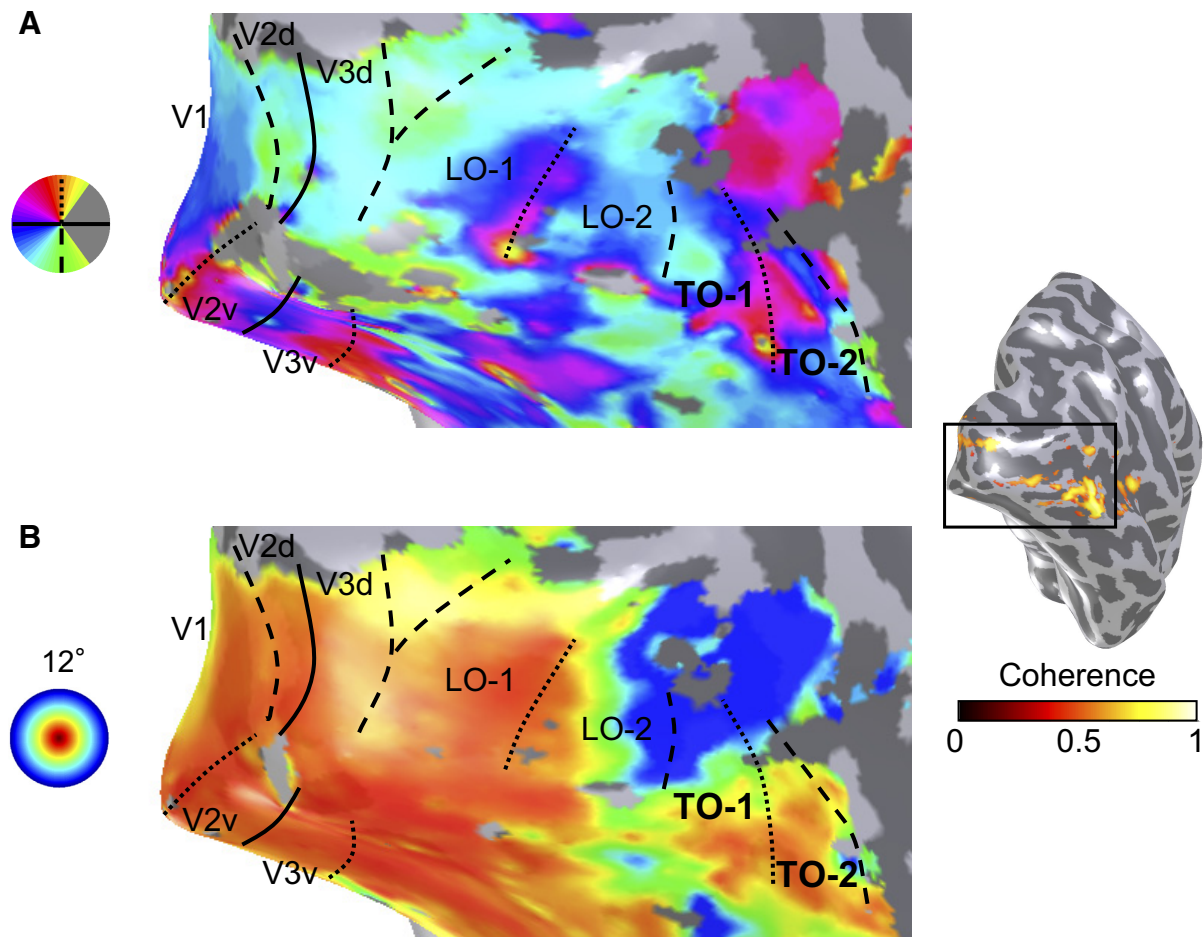
FIG. 1. Temporal–occipital (TO) visual field maps in a right hemisphere. The data shown are from one subject (S2) with a particularly clear visual field map organization. The data are shown on the subject's own inflated cortical surface. The *inset* at the *right* shows the motion-selective middle temporal area (MT+) localizer responses; the black rectangle indicates the region of posterior temporal–occipital cortex that is shown in a more detailed view in the *left panels*. *A*: angle maps. The legend shows the relationship between color and the most effective stimulus angle. The temporal–occipital cortex (lower to upper vertical meridian, TO-1) has a peak response to angles near the lower vertical meridian on its posterior side at the boundary with the lateral occipital cortex (upper to lower vertical meridian, LO-2). The angular representation of TO-1 continues through horizontal toward the upper vertical meridian at the boundary with TO-2 and the TO-2 angle map reverses. Light and dark shaded regions of the cortical surface indicate gyri and sulci locations, respectively. *B*: eccentricity maps. The legend shows the relationship between color and most effective eccentricity. Two distinct foveal confluences are present. The foveal representation for V1/V2/V3/LO-1/2 is posterior (*left*) compared with the TO-1/2 foveal representation. In the TO-1/2 maps, eccentricity increases from ventral to dorsal.

of these areas, we refer to the anterior maps in temporal–occipital cortex as TO-1 and TO-2.

The TO-1 angle map extends from the lower visual field, at the boundary with LO-2 (Larsson and Heeger 2006), through the horizontal meridian to the upper visual field, at the boundary with TO-2. The angle map for TO-2 is a mirror image of TO-1; it extends from the upper to lower visual field. The angle map reversals define the borders between LO-2/TO-1 and TO-1/TO-2 for each individual subject, but quality of the maps varies across subjects. We observed these borders in 10/14 and 13/14 hemispheres, respectively (see Table 1). The criterion is whether there is a reversal of angle representation clearly detectable by eye. The difficulty in defining the LO-2/TO-1 border comes from the inability to identify LO-1/2 maps (2/14) or from the presence of angle intermixed responses; that is, in addition to the expected vertical meridian response there were also some responses to the opposite vertical meridian or the horizontal meridian (2/14).

Although the border between the two TO maps is evident in almost all (13/14) hemispheres, some individual TO-2 maps

are incomplete and their anterior border represents the horizontal rather than the lower vertical meridian. In 9 of 14 hemispheres the TO-2 visual field representation responded to visual stimuli from both the upper and lower visual field, whereas the other maps (e.g., S1 left and S5 left in Fig. 2) end on the horizontal rather than the lower vertical meridian (see Table 1).

The eccentricity map shows that the TO-1/2 maps form a confluent foveal representation; in most subjects this foveal confluence is separate from that of V1/2/3 and LO-1/2. In both TO-1 and TO-2 maps eccentricity increased from ventral to dorsal. In 4 of 14 hemispheres, including both hemispheres of S3 and the left hemisphere of S5 (Fig. 2), the foveal representation is contiguous with the early visual areas (see Table 1).

The LO-1 angle map extends from the lower visual field, at the boundary with V3d, through the horizontal meridian to the upper visual field, at the boundary with LO-2. The LO-2 angle map extends from the upper to lower visual field (Larsson and Heeger 2006). The V3d/LO-1 and LO-1/LO-2 borders were observed in 13/14 and 9/14 hemispheres, respectively (see
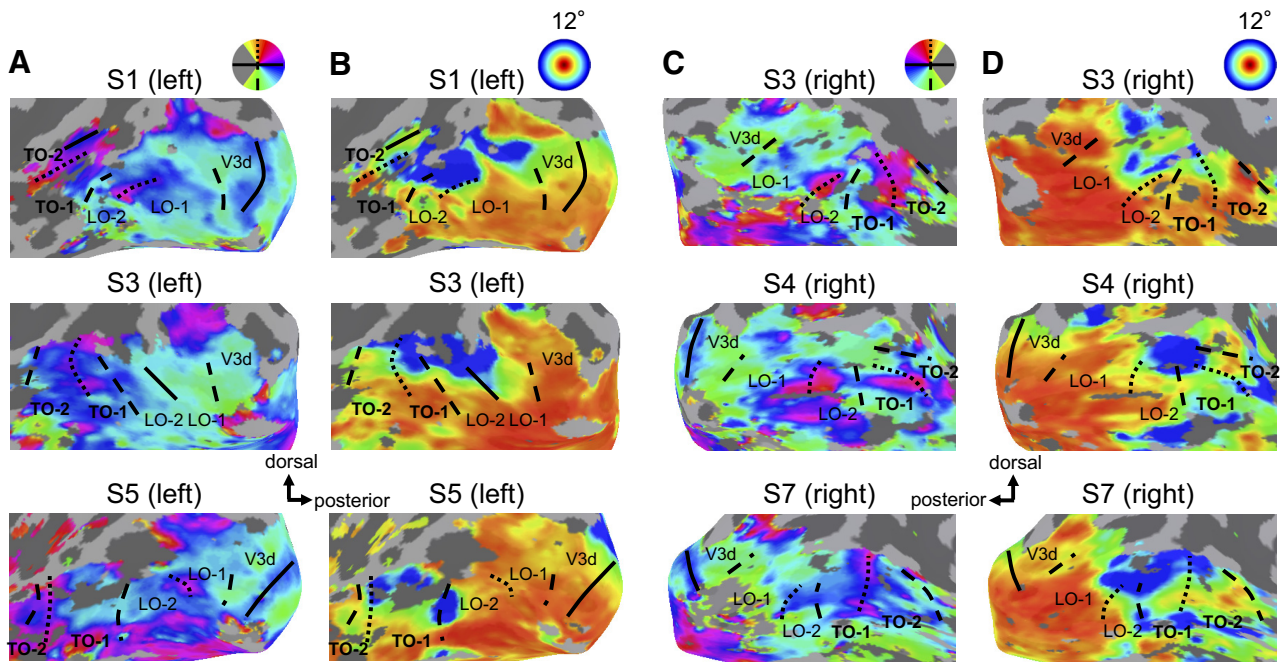
FIG. 2. Temporal–occipital visual field maps in 6 additional hemispheres. The data shown are from 6 hemispheres chosen to illustrate the variation between subjects (all subjects are shown in Supplemental Figs. S1, S2, S5, and S6). Each data set is shown on the subject's own inflated cortical surface. Other details are as in Fig. 1. Anterior border of some TO-2 maps (e.g., S1 left and S5 left) represents the horizontal rather than the lower vertical meridian. TO-1/TO-2 fovea were not separated from V1/V2/V3/LO-1/2 for some hemispheres (e.g., S3 left, right and S5 left). See Table 1 for detail of the variance with respect to several map landmarks.

Table 1). The difficulty in defining the LO-1/LO-2 border comes from lack of upper vertical meridian (3/14) or from the intermixed angle representations (2/14). The ability to identify these boundaries is consistent with a previous study that reports only half of the hemispheres showed clear hemifield representations (Larsson and Heeger 2006).

Average TO maps

To increase the power of the measurements, we aligned and averaged the visual field maps across subjects (see METHODS for details).

Figure 3, *A* and *B* shows the angle and eccentricity maps averaged across all 14 hemispheres. There is great regularity in the representation combined across subjects, so that the reversals in the angle maps are quite evident (Fig. 3*A*). The figure shows both angle and eccentricity maps derived for V1/2/3 and LO/TO maps using the same methods. We made two separate flattened cortical representations to avoid the deformations associated with very large flattened regions. These V1/2/3 results confirm the well-known angle reversals between the maps and the expanded representation of the near foveal region. The pooled representation confirms the presence of four additional visual field angle maps beyond V3d whose borders are defined by a reversal of the change in angle. TO-1/TO-2 share an eccentricity representation that is distinct from the one shared by V1/V2/V3 and LO-1/LO-2.

TABLE 1. *Summary of observer variance with respect to several map landmarks*

Subject	R/L	V3d/LO-1 (Lower)	LO-1/LO-2 (Upper)	LO-2/TO-1 (Lower)	TO-1/TO-2 (Upper)	TO-2 Anterior (Lower)	Separate TO-1,2 Fovea
S1	L	○	○	○	○	Horizontal	
	R	○	○	○	○	Horizontal	○
S2	L	○	○	○	○	○	○
	R	○	○	Intermixed	○	Horizontal	○
S3	L	○	○	○	○	○	
	R	○	No upper	No LO	○	○	
S4	L	○	○	○	○	○	○
	R	○	Intermixed	○	○	○	○
S5	L	○	○	○	Intermixed	○	○
	R	○	○	○	○	Horizontal	
S6	L	○	○	○	○	○	○
	R	Intermixed	Intermixed	Intermixed	○	Horizontal	○
S7	L	○	No upper	No LO	○	○	○
	R	○	No upper	○	○	○	○
Number		13/14	9/14	10/14	13/14	9/14	10/14

The table shows whether each landmark is clearly definable (○) or how it is not clear. "Intermixed" indicates that in addition to the expected vertical meridian response there were also some responses to the opposite vertical meridian or the horizontal meridian.

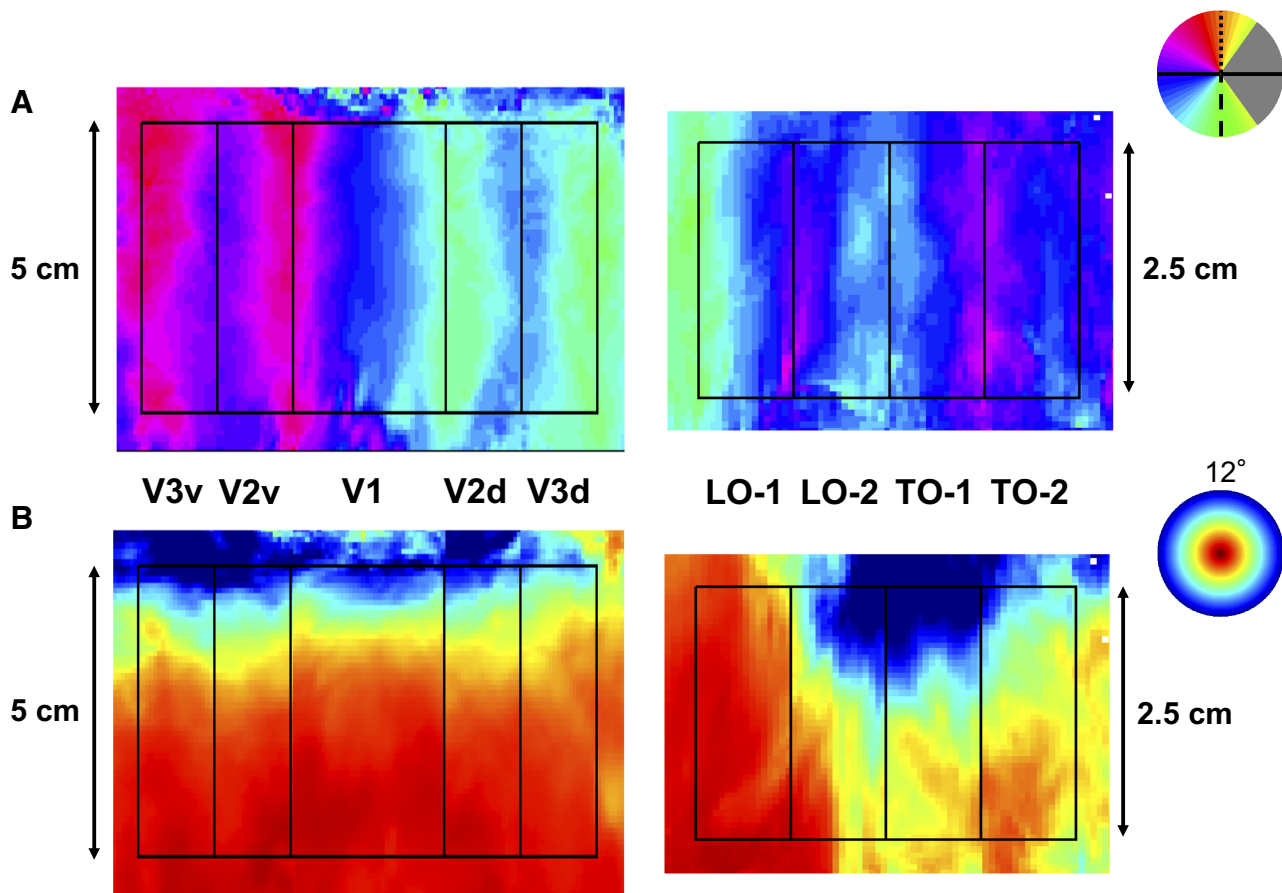**V3v V2v V1 V2d V3d**   **LO-1 LO-2 TO-1 TO-2**

FIG. 3. Average angle and eccentricity maps. The individual maps were transformed into a common atlas space and averaged across all 14 hemispheres. *A*: averaged angle maps. Angle reversals are evident at the boundaries. Peak angles in LO-1/2 and TO-1/2 fall within both the lower and upper visual fields. *B*: averaged eccentricity maps. TO-1 and TO-2 share a foveal representation that is distinct from that of LO-1/2. LO-1 mostly represents the foveal region. The angle and eccentricity maps are not orthogonal in LO-2 and TO-1/2. Approximate length of the atlas of visual cortical areas V1–V3 (5 cm) was obtained by averaging the cortical distance of V1 representing horizontal meridian. Approximate length of the atlas of LO and TO (2.5 cm) was obtained by averaging all 5 borders of maps across all subjects.

There is a valid concern with the atlas-based averaging procedure. Could the atlas-based averaging method impose the retinotopic outcome when the data are not retinotopic? For three reasons, we do not believe this is the case. First, the atlas-based averaging did not re-create the template. For example, the angle and eccentricity representations are orthogonal in the template, although the derived angle and eccentricity maps are not orthogonal in LO and TO. Second, we performed two computational experiments in which we applied atlas-based averaging to *1*) anatomical regions anterior to TO, where we could not discern maps in individual brains (one edge on TO-2 and the second edge ~1 cm anterior and parallel to the edge of TO-2); and *2*) to noisy regions without identifiable retinotopic features (Supplemental Figs. S9 and S10). In both cases, the sizes of the regions were comparable to the TO-1/2 map sizes and the data were taken from all subjects and hemispheres, as in our main analysis (Fig. 3). Applying atlas-based averaging in these cases did not produce complete visual field maps. Third, we note that the experimental results have an independent empirical test of the map validity: the localizer responses coregister with specific maps (see following text). The spatial correspondence between these stimulus-selective responses and the maps further supports the functional validity of the derived maps. Therefore we conclude the atlas-based averaging method performs averaging correctly: the method

removes noise from existing maps and does not create maps de novo from noise.

The LO-1 and LO-2 maps we measured confirm many aspects of the previous reports (Larsson and Heeger 2006): *1*) the LO-1 and LO-2 maps are located in the fundus of the lateral (middle) occipital sulcus, *2*) the eccentricity range in the LO-1 map is smaller than the range in the LO-2 map, and *3*) the eccentricity and angle maps are not orthogonal. The measurements differ mainly in the estimated LO pRF sizes (see following text).

A salient feature of the LO and TO maps is that the angle and eccentricity representations are not perpendicular. This feature appears in the combined maps, even though the templates we used to identify the maps assume that the angle and eccentricity representations are perpendicular. Tyler and Wade (2005) commented on this issue broadly, explaining that angle and eccentricity representations do not need to be perpendicular but should be nonparallel, to provide a point-to-point mapping of the visual field. This feature was specifically measured in LO-2 by Larsson and Heeger (2006) who estimated that the mean angle between the angle and eccentricity maps is 15.3°, but significantly different from 0 (parallel). Despite the nonperpendicular orientation of the angle and eccentricity representations, the pooled response of voxels within each of these maps does respond to stimuli placed anywhere within a visual

K. AMANO, B. A. WANDELL, AND S. O. DUMOULIN

TABLE 2. *Surface area size (mm^2) of LO-1/2 and TO-1/2*

	LO-1	LO-2	TO-1	TO-2
Left				
Mean	248	329	277	226
Range	156–416	241–522	154–510	118–395
Right				
Mean	313	249	238	303
Range	200–476	151–362	167–306	200–435
Mean				
Mean	281	289	258	265
Range	189–446	228–347	174–387	169–319

hemifield. We demonstrate this coverage in Fig. 7 in the following text.

The representation shown in Fig. 3*A* illustrates the most effective stimulus angle (peak angle). This estimate does not span a full hemifield representation in the LO and TO maps, but rather is confined to a limited range above and below the horizontal meridian. There are several reasons for the limited range of the estimated peak angle. First, voxels at the vertical meridian representation include cells that are most responsive to angles that are away from the vertical meridian, closer to the horizontal meridian. Thus averaging near the border generally produces angle estimates that are biased toward the horizontal meridian; this effect is amplified when the area size is small and the pRF is large. Second, pooled estimates are also biased toward reducing the full hemifield representation. Imperfections in the area alignment will always bias the mean peak angle toward the horizontal meridian. Finally, despite the small peak angle range, we show later that these maps cover a hemifield when pRF size is incorporated (Fig. 7). Consistent

with these arguments, the V1/2/3 angle maps also have limited range, not reaching all the way to the upper and lower vertical meridians.

Each of the TO maps occupies a small surface area

We measured the cortical surface area of the central 10° of LO-1/2 and TO-1/2 (Table 2).

The surface areas of the four LO and TO maps are comparable (250–290 mm^2). These maps are all much smaller than those of V1/2/3 (Dougherty et al. 2003), so that the central 10° representation of LO and TO maps occupies about one fifth of the corresponding V1 surface area. Although the TO-1/2 and LO-2 maps cover nearly the central 10°, the LO-1 map does not include peak eccentricities beyond about 5°. Thus evaluating the surface area per square degree of visual field would amplify the LO-1 representation.

TO maps have expanded foveal representations

Figure 4 shows the eccentricity of the pRF center estimate (peak eccentricity) as a function of cortical surface location. The four panels show the LO and TO functions. The points with a common symbol are measured from a single hemisphere.

Within each hemisphere data were analyzed along isoangle lines specified by the atlas-fitting procedure (Dougherty et al. 2003) (see METHODS for details). The data points represent cortical position (*D*) in millimeters and visual field eccentricity (*E*) in degrees. The initial distance *D* measures the distance from the 1° position in the atlas. The functions along each isoangle line are binned together
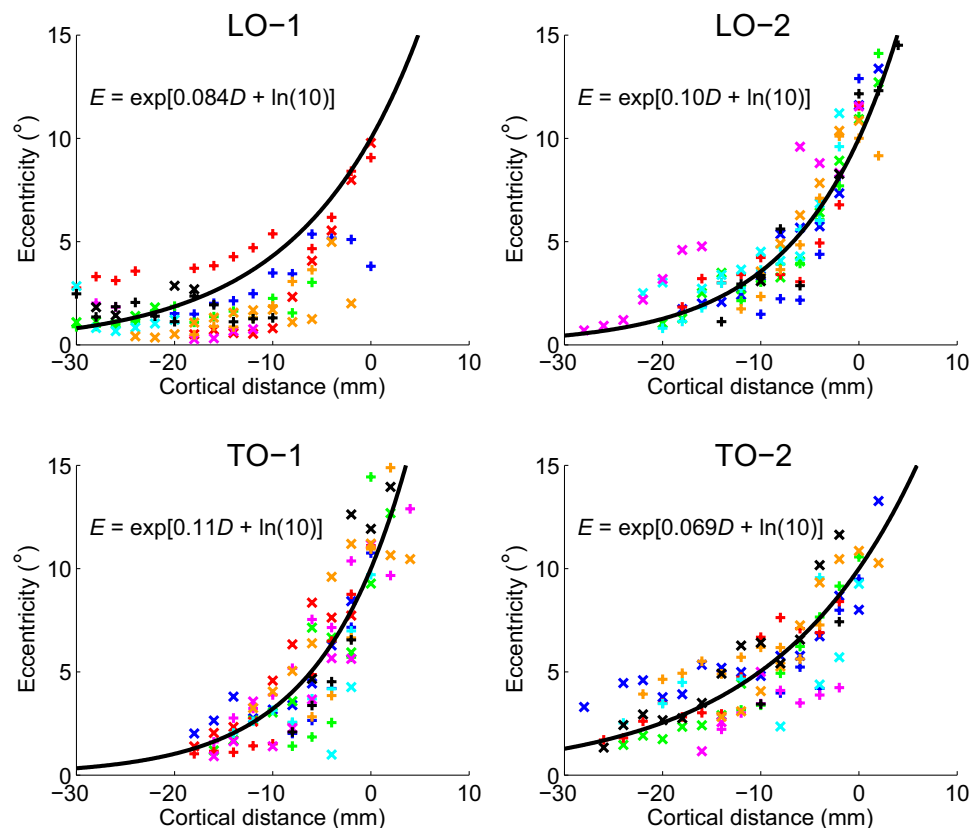

FIG. 4. Cortical magnification in the LO and TO maps. The most effective eccentricity is shown as a function of cortical distance. Separate panels plot the functions for LO-1/2 and TO-1/2. The data are aligned at the 10° eccentricity point. For each hemisphere, eccentricity was measured along 4 isoangle lines, derived from the atlas procedure (see METHODS for details), and averaged across these lines. Cortical distances are grouped into bins and the average eccentricity within each bin was computed. Each color represents a different subject and each symbol type represents the left (+) or right (×) hemisphere. The smooth curve is the best (least-squares) fit to the data; the equation of the fit is shown in each panel where *E* is the eccentricity (degrees) and *D* is the cortical distance (mm).

and fit by an exponential function of the form $E = \exp[s(D - d_0) + \ln(10)]$. In this function, s is a scaling parameter and d_0 permits translation of the distance scale. After obtaining the best fit for a single hemisphere, we translate the distances so that at $D = 0$ the value of E is 10°.

The general form of the function for all subjects and field maps is similar. The LO and TO maps have an expanded foveal representation, similar to that of V1/2/3 (Engel et al. 1997; Larsson and Heeger 2006; Sereno 1995). We fit the combined data from all hemispheres by a single exponential (solid line) to obtain a summary scale factor s. The scale factors for the LO-2 and TO-1 visual field maps are near 0.1, whereas those for LO-1 and TO-2 are slightly smaller (0.084 and 0.069, respectively). These values are larger than the values for V1/2/3, which are near 0.06 (Supplemental Fig. S11). The difference in the scaling factor between the TO maps and the V1/2/3 maps is qualitatively consistent with the smaller size of the TO maps.

The curves for individual hemispheres and subjects differ. We do not think these differences are due to noise, but rather they reflect genuine individual variability in the size and compression of the visual field representation within these maps (see Table 2) (Duncan and Boynton 2003).

pRF sizes in TO exceed 5°

The pRF method provides an estimate of pRF size as well as center location. The pRF size estimates from one subject (S2) and estimates derived by combining data across subjects are shown in Figs. 5 and 6, respectively.

The pRF size estimates are based on the measured difference in the BOLD time course responses. The time series shown in Fig. 5A illustrate the responses to a rotating wedge stimulus with four blank periods (blue bars). There is an enormous difference between the time courses in V1 and TO-2. These differences cannot be explained by differences in the HRF functions (Dumoulin and Wandell 2008). The V1 responses reach a peak of 3% when the wedge is in a narrow range of angles, dropping to baseline otherwise. The TO-2 responses are high whenever the wedge is present, dropping to baseline only during the blank periods. The differences in these responses are captured by the pRF method and are explained by differences in the pRF size (Dumoulin and Wandell 2008).

The estimated pRF size increases systematically, and substantially, from V1/2/3 through LO-1/2 and TO-1/2. The colors on the cortical surface in Fig. 5B represent the size (σ) of the fitted Gaussian pRF. For this subject, the pRF size increases from <1° in V1/2/3 to between 8 and 12° in TO-1/2.
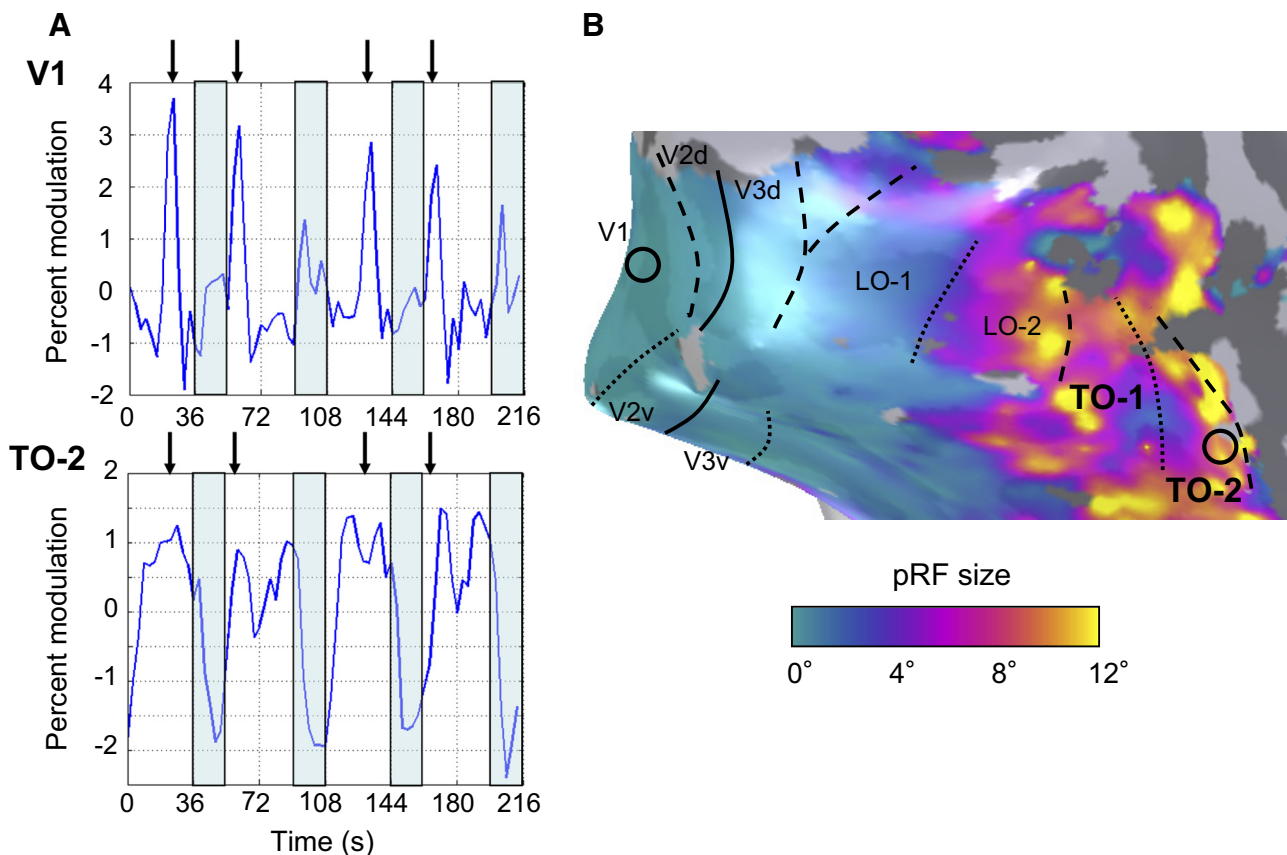

FIG. 5. Population receptive field (pRF) size map in a right hemisphere (S2). *A*: the time-series responses to a rotating wedge stimulus with inserted blanks (mean-luminance) from a region of interest in V1 (*top*) and TO-2 (*bottom*) are shown. The locations of these regions are shown by the circles on the inflated cortical surface (*B*). The vertical arrows indicate the strongest functional magnetic resonance imaging (fMRI) response elicited by the same wedge orientation. Light blue regions indicate the mean-luminance blocks. The 2 cortical locations responded maximally to roughly similar wedge positions. In V1, little fMRI modulation is observed by the insertion of mean-luminance blocks. In TO-2, every insertion of mean-luminance blocks causes a drop in the blood oxygen level–dependent modulation, demonstrating that TO-2 is responsive to all wedge orientations. These differences are explained mainly by differences in the pRF size (Dumoulin and Wandell 2008). *B*: the pRF size is shown on the subject's inflated cortical surface. The color overlay shows the estimated pRF size (σ). There is a progressive increase in pRF size from V1 to TO-2. The pRF size in V1/V2/V3/LO-1 is <3°, whereas the size in TO-1/2 exceeds 10°.

Figure 6 quantifies the increase in pRF size in two ways. Figure 6*A* shows the relationship between pRF size and eccentricity, averaged across all 14 hemispheres. Within each map the pRF size increases with eccentricity almost linearly. Further, there is a progressive increase in the pRF size from V1/2/3 to LO-1/2 and TO-1/2, with the largest pRF sizes in TO-2. The slopes of the fitted lines for LO-1/2 and TO-1/2 are almost the same and steeper than the corresponding slopes for V1/2/3.

Figure 6*B* shows the pRF size data again combined across subjects, for LO, TO, and V1/2/3. The increase in pRF size across the maps is clearly evident; on close inspection it is possible to see the increasing size with eccentricity within each map, as well.

Estimates of LO-1/2 pRF sizes are larger than the Larsson and Heeger (2006) estimates. For example, we estimate that LO-1/2 pRF sizes range from 2 to 8° and increase with eccentricity; Larsson and Heeger (2006) estimate LO-1/2 pRF sizes to be <1°, similar to the size of V1 pRF sizes. In our earlier study (Dumoulin and Wandell 2008) we demonstrated that duty-cycle–related measures with conventional stimuli like those reported by Larsson and Heeger (2006) cannot distinguish very large pRF responding to all stimulus locations to various degrees versus small pRF responding to only a few stimulus locations because of the missing baseline. We show in that study that the insertion of mean-luminance blocks (baseline) is crucial to measure large pRF sizes. We believe the missing baseline in Larsson and Heeger (2006) led them to systematically underestimate the pRF sizes.

TO maps extend into the ipsilateral visual field

The visual field coverage of the voxels within each map depends on both the pRF centers and sizes. To estimate the visual field coverage of a map, we combine the pRF from every voxel in every subject. Since the asymmetry between right and left hemispheres was not substantial (Supplemental Figs. S12 and S13 for left and right hemispheres, respectively), we combine the data across both hemispheres. The four panels in Fig. 7 compare the visual field coverage in V1, V3v, TO-1, and TO-2. There are two plots within each panel. The image on the *left* shows the positions of the pRF centers and the image on the *right* shows the visual field coverage obtained by combining the pRF centers and sizes (see METHODS for details).

In V1 the pRF centers span most of a hemifield. There are fewer pRF centers for the periphery because in most subjects the stimuli covered only the central 10°. Accounting for both the centers and pRF size, the visual field coverage is mainly confined to a hemifield. The coverage into the ipsilateral visual field is modest, extending perhaps 2°. Even this coverage may be an overestimate that can be explained by the use of a circularly symmetric Gaussian model for the pRF. If we allow an asymmetric model, the ipsilateral coverage might be reduced.

The V3v pRF centers are confined to a quadrant, as expected. The coverage extends slightly beyond the quadrant, but again this may be due to inadequacies of the pRF model shape.

The pRF centers in TO-1/2 do not extend across a broad range; for example, they do not reach either vertical midline. However, when we account for the large pRF size the visual
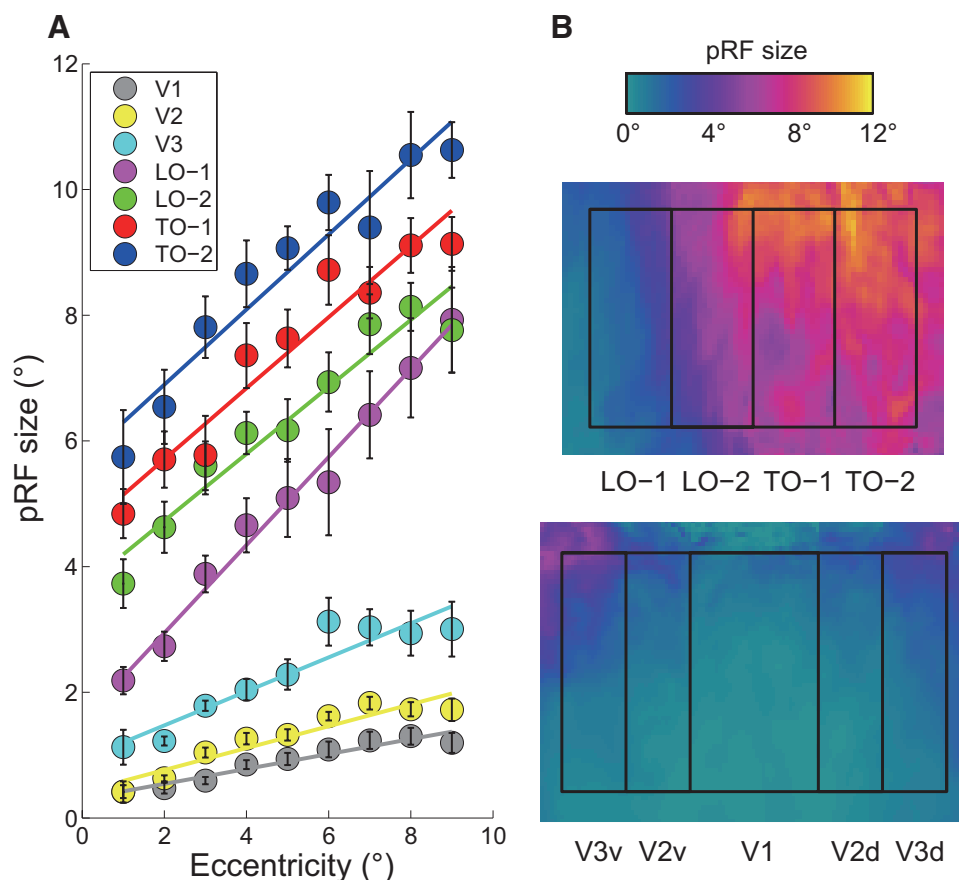

FIG. 6. The relation between pRF size and eccentricity and the average pRF size map. *A*: averaged pRF size (σ) as a function of eccentricity for all identified visual field maps. The pRF size increase from V1/2/3 to LO-1/2 and TO-1/2. Within each visual field map, pRF size increases linearly with eccentricity. *B*: the individual pRF maps were averaged across all subjects in a common atlas space. The color overlay shows the pRF size (σ). Both the increase in pRF size across maps and the eccentricity-dependent increase in pRF size within each map (from *bottom* to *top*) are observable.
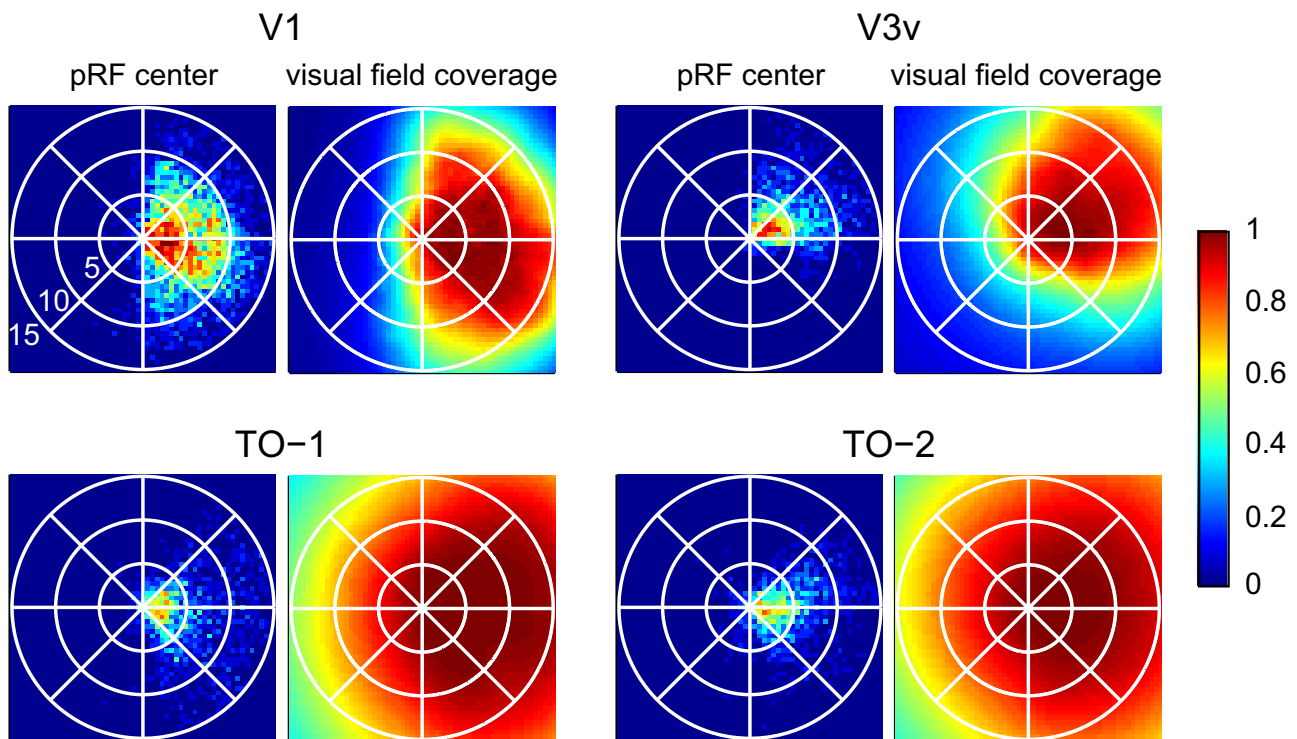
FIG. 7. Averaged pRF center distribution and visual field coverage. The separate panels show measurements from V1, V3v, TO-1, and TO-2. The *left panels* show the distribution of pRF centers; the *right panels* incorporate the pRF sizes in the computation of the visual field coverage (see METHODS for details). The data are combined across all subjects and hemispheres. The data from the right hemisphere were converted into left-hemisphere format to pool across both left and right hemispheres. As expected, the V1 and V3v coverage is mainly confined to the contralateral hemifield and contralateral upper quadrant, respectively. The visual field coverage in TO-1 and TO-2 spans the entire contralateral hemifield but extends significantly into the ipsilateral visual field. The ipsilateral extension of TO-2 exceeds that of TO-1, mainly because of the larger pRF sizes; the pRF center distributions are similar. In individual subjects, the TO-1/2 visual field coverage also spans the entire contralateral hemifield.

field coverage within the TO maps extends across a full hemifield and into the ipsilateral field. Although the pRF centers distributed similarly in TO-1 and TO-2, the ipsilateral coverage in TO-2 is greater than that of TO-1, mainly due to the larger pRF sizes. The pRF center distributions and visual field coverage of all identified maps are available in Supplemental Figs. S14 and S15, respectively.

The difference in visual field coverage between TO-1 and TO-2 (~5°) is larger than the difference in mean pRF size (~1–2°, Fig. 6*A*). This is because the visual field coverage is formed by the maximum coverage of all individual pRF estimates; this coverage is influenced more by the largest pRF sizes.

TO and LO maps correspond to regions identified by motion and object localizers

The human motion-selective complex MT+ is identified by contrasting moving and stationary stimuli (Tootell et al. 1995; Watson et al. 1993; Zeki et al. 1991). The stimulus is presented over a region that spans the central visual field. The response to this localizer coincides well with the visual field maps, TO-1 and TO-2, as is shown in subject S2 (Fig. 8*A*) and the average across subjects (Fig. 8*B*). The MT+ localizer (foveal motion) produces a BOLD response in multiple locations, including the foveal representation of LO-1/2, but the amplitude is weaker. In separate experiments (Supplemental Figs. S3 and S7) we found that a motion stimulus in the contralateral peripheral visual field (>10°) produces a powerful TO-1/2 response with a much

reduced response in LO-1/2 and other cortical locations. This is consistent with the relatively large pRF sizes in TO-1/2 compared with other cortical regions (Fig. 6).

Motion-selective cortex (MT+) borders an object-selective region known as the lateral occipital complex (LOC) (Grill-Spector and Malach 2004; Malach et al. 1995). LOC is identified by contrasting intact and scrambled objects. The response to the LOC localizer falls in the adjacent, relatively posterior region of cortex that includes LO-2, as shown in subject S2 (Fig. 8*C*) and the average across subjects (Fig. 8*D*).

Previous studies subdivided MT+ into two subregions by measuring responses to peripheral motion stimuli (>10°) (Dukelow et al. 2001; Huk et al. 2002). They found stronger ipsilateral responses in an anterior part of MT+, compared with the posterior part. This distinction coincides well with TO-2, as is shown in subject S2 (Fig. 8*E*) and the average across subjects (Fig. 8*F*). The data of all 14 hemispheres are available in Supplemental Figs. S4 and S8. It was proposed that this subregion is the human homologue of macaque MST (Dukelow et al. 2001; Huk et al. 2002).

DISCUSSION

Related human MT+ studies

The original definition of area MT in owl monkey was based on the discovery of a visual field map, but it has proven difficult to measure visual field maps in human MT+. Previous
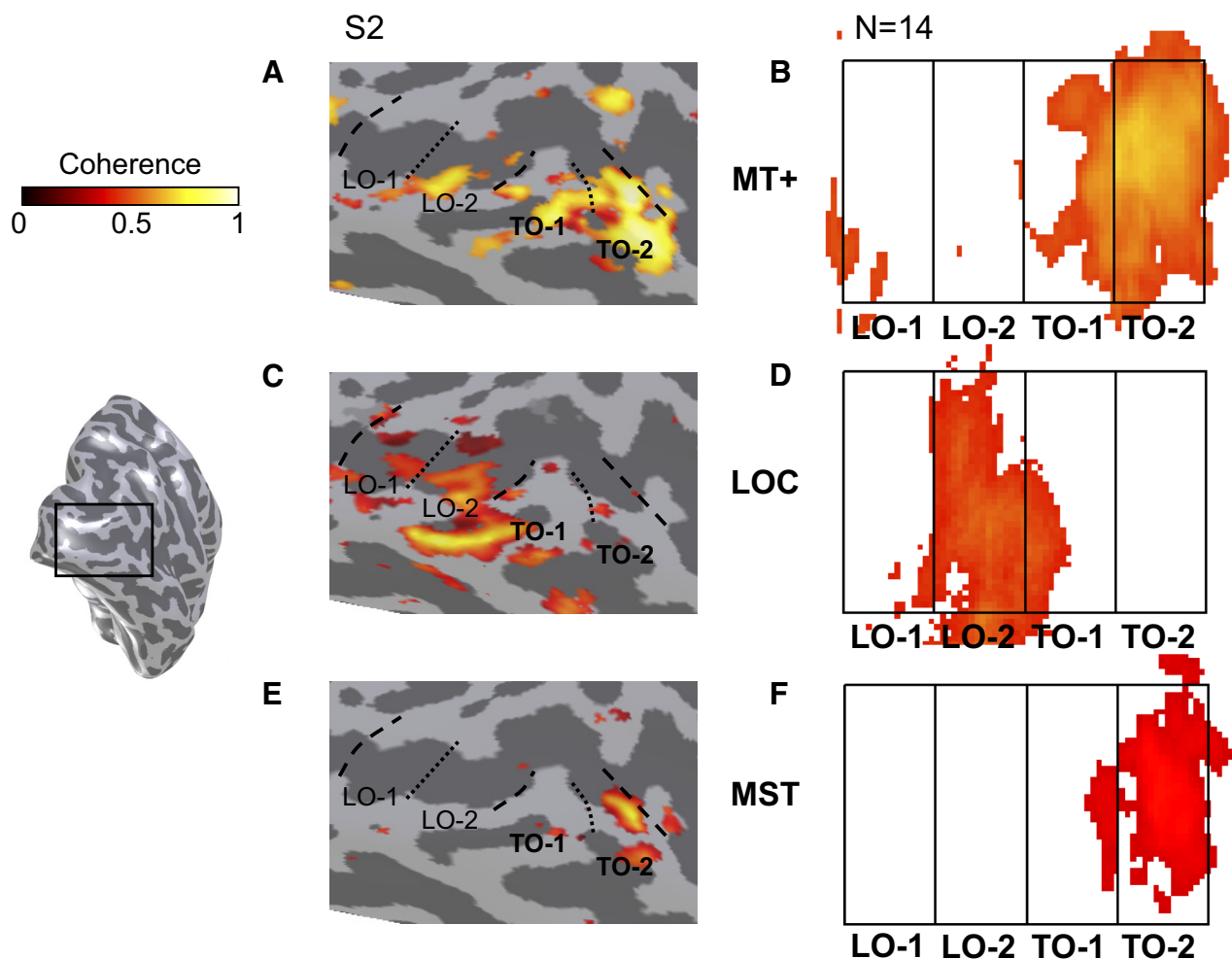
FIG. 8. The relationship between visual field maps and conventional functional localizers. The responses for subject S2 (*A*, *C*, *E*) and averaged responses from 14 hemispheres (*B*, *D*, *F*) are shown. The *inset* at the *left* shows a posterior view of the subject's inflated cortical surface. The black outline indicates the region shown in *A*, *C*, and *E*. The *top panels* (*A* and *B*) show that the strongest responses to the MT+ localizer coincide with TO-1 and TO-2 (coherence >0.6 for S2 and coherence >0.4 for the average). The *middle panels* (*C* and *D*) show that the strongest responses to the lateral–occipital complex (LOC) localizer coincide with LO maps, in particular LO-2, but not the TO maps (coherence >0.4 for S2 and the average). The *bottom panels* (*E* and *F*) show that the strongest responses to the MST localizer is confined mainly to TO-2 (coherence >0.4 for S2 and coherence >0.3 for the average). The response to the medial superior temporal area (MST) localizer was weak and therefore the threshold for the average response may is lowered. The presented data are highly significant (*P* < 0.01, corrected).

studies succeeded in measuring differences in the locations of responses to upper and lower vertical stimuli within the posterior portion of MT+ (Huk et al. 2002; Saygin and Sereno 2008). These studies did not report reliable eccentricity maps, but the trends in their data (Huk et al. 2002) were consistent with the MT maps in monkey. We note that these studies failed to define a map in the anterior region corresponding to MT+.

Using the new methods we find that MT+ has two visual field maps: TO-1 and TO-2. The angular representation of TO-1 continues through the horizontal to the upper vertical meridian at the boundary with TO-2, and the TO-2 angle map reverses from upper to lower visual field at increasingly anterior positions. TO-1/TO-2 share a parallel eccentricity map in which central to peripheral runs from ventral to dorsal with an expanded foveal representation.

Previous fMRI studies (Dukelow et al. 2001; Huk et al. 2002) partitioned MT+ based on functional responses, not on retinotopy. Specifically, they found that responses in posterior MT+ are confined to stimuli in the contralateral visual field or

stimuli near the vertical midline (Tootell et al. 1995), whereas the anterior part responds to ipsilateral as well as contralateral stimuli. The posterior and anterior parts of MT+ are tentatively called MT and MST, respectively (Dukelow et al. 2001; Huk et al. 2002). We confirmed that MT+ localizer activates both TO-1 and TO-2 and that the peripheral portion of TO-2 responds well to ipsilateral motion in the visual periphery. Thus it is likely that TO-1 corresponds to their MT, whereas TO-2 includes the region identified by previous authors as MST. The subregion of MT+ sensitive to circular or radial optic flow is reported to be distinct from the subregion sensitive to translational motion (Morrone et al. 2000), but the relationship of these measurements to TO-1/TO-2 maps is not clear in our experiments since we used only radial motion as a functional localizer.

Visual field maps are a relatively secure way to partition MT+ because the method avoids biases that arise from localizers. For example, MT+ localizers are sometimes based on moving dots that form an optic flow pattern. In this case the

localizer may be biased toward identifying TO-2 (MST) voxels because of the well-known responsivity of MST voxels to such patterns. In other cases, MT+ is localized using drifting gratings. In this case the localizer may be biased toward TO-1 (MT) voxels. Identifying the region based on visual field maps eliminates this bias.

Several studies have reported that human MT+ responses have direction selectivity (Huk et al. 2001), a linear increase in amplitude with motion coherence (Rees et al. 2000), or sensitivity to pattern motion rather than to component motion (Huk and Heeger 2002). The spatial distribution of these responses can be revisited now that it is possible to distinguish TO-1 and TO-2 regions within MT+.

Anatomically, area MT can be identified as the heavily myelinated portion of the striate (V1) projection field in the superior temporal sulcus (Desimone and Ungerleider 1986; Maunsell and Van Essen 1983; Tootell and Taylor 1995). A previous study used high-resolution structural MRI in human to identify distinct cortical regions based on cortical lamination structure (Walters et al. 2003). They demonstrated that the observed MR lamination patterns relate to myeloarchitecture through a correlation of histology with MRI and could identify MT. The comparison between this definition of MT and our definition of TO-1 would be interesting in the future.

Our size estimates of TO-1 and TO-2 are comparable to previous estimates. By staining the postmortem human brain, Tootell and Taylor (1995) estimated that human area MT has a surface area of 228 mm^2. Dukelow et al. (2001) estimated the volume of MT as 1 cm^3; assuming a cortical thickness of 2.5–4 mm this is a surface area of about 250–400 mm^2. Huk et al. (2002) estimated the MT surface area to be 243 mm^2. We estimate that the portion of TO-1 that represents the central 10° spans 258 mm^2. These four estimates of the TO-1 (MT) surface area are in good agreement. The surface area of MST is estimated to be considerably smaller than that of MT (Dukelow et al. 2001; Huk et al. 2002). The former describes a volume of 0.380 cm^3 (surface area 100–160 mm^2), whereas the latter estimated a surface area of 83 mm^2. We estimate the TO-2 (MST) representation of the central 10° to be 265 mm^2, larger than the other estimates. The previous study commented that their values "are likely to be underestimates, because of the conservative criteria used in defining this area" (Huk et al. 2002).

Comparison between TO-1/TO-2 and MT/MST in macaque monkey

Primate visual area MT and neighboring areas such as MST and FST are vital for motion perception (Desimone and Ungerleider 1986; Komatsu and Wurtz 1988; Maunsell and Van Essen 1983). About 90% of MT neurons are direction-selective (Desimone and Ungerleider 1986) and their firing rate is correlated with perceived motion (Britten et al. 1992, 1996). Microstimulation of MT neurons biases motion-direction judgments (Salzman et al. 1992). MST, which receives inputs from MT neurons (Ungerleider and Desimone 1986), is typically divided into a dorsal region (MSTd) and a lateral–ventral region (MSTl). The neurons in MSTd have a much larger receptive field than that of neurons in MT and respond strongly to optic flow stimuli (Duffy and Wurtz 1991). Neurons in the nearby region, MSTl, may have a role in segmenting motion of a small object from background (Eifuku and Wurtz 1999; Tanaka

et al. 1994). FST has fewer direction-sensitive cells and receives input from V4, which MST lacks (Boussaoud et al. 1990).

The TO-1 visual field map response properties are roughly consistent with the monkey MT responses measured with single-unit recordings (Desimone and Ungerleider 1986; Komatsu and Wurtz 1988; Maunsell and Van Essen 1983) and with fMRI (Brewer et al. 2002; Fize et al. 2003; Orban et al. 2004; Vanduffel et al. 2001). Specifically, several studies report that the posterior and anterior parts of MT represent lower and upper visual fields, respectively, and the eccentricity increases from ventral to dorsal. Also, in monkey MT the lower visual field is overrepresented compared with the upper visual field (Maunsell and Van Essen 1987). This overrepresentation can be detected using fMRI in macaque (Brewer et al. 2002). The distribution of pRF centers (Fig. 7, *left panels*) suggest that the representation bias might also exist in human, although the bias was not observed in earlier human fMRI analyses of motion-selective cortex (Tootell et al. 1995). There is a difference, however. The receptive field size estimates in TO-1 are substantially larger than the estimates in monkey MT. For example, there is consensus that the MT receptive fields in macaque, at roughly 5° eccentricity, span 5–7° (Felleman and Kaas 1984; Komatsu and Wurtz 1988; Maunsell and Van Essen 1987). The pRF radius (σ) estimates for TO-1 at 5° eccentricity are 7–8° (Fig. 6A). Assuming the reported receptive field size in monkey corresponds to the full width half-maximum of our Gaussian pRF, our estimates of 7–8° radius are equivalent to a population receptive field width of 15°. Thus the human TO-1 pRF sizes are two to three times the size of the monkey MT receptive fields.

For two reasons, we speculate that the TO-2 visual field map mainly corresponds to macaque MSTl not MSTd. First, using electrophysiology, some authors describe visual field maps in MST (Desimone and Ungerleider 1986; Komatsu and Wurtz 1988) and report that MSTl shares fovea with MT, whereas MSTd does not (Komatsu and Wurtz 1988). The TO-2 location and map are roughly consistent with the MSTl map. Second, receptive fields in macaque MSTd have a width of 30–50° that is indepen-
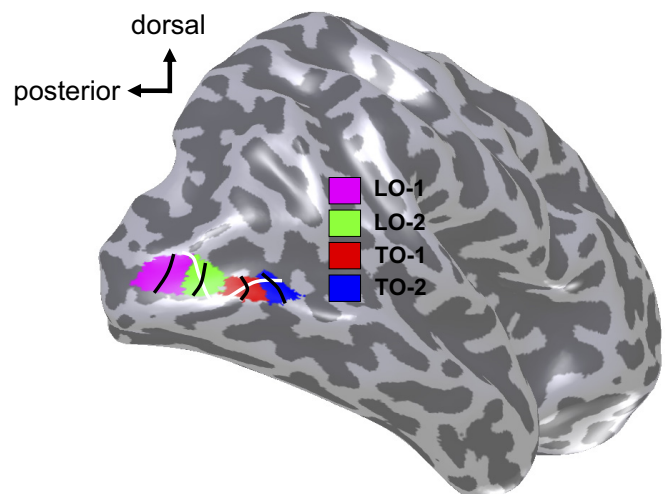

FIG. 9. A model of the sequence of maps on the lateral surface. Each colored region represents a visual field map on the lateral surface. The black lines indicate the horizontal isoangle contours of each map; that is, the region most powerfully driven by signals along the horizontal meridian. The white line indicates the isoeccentricity contour (6°) for each map. The model is based on individual subject data (S2).

dent of eccentricity (Raiguel et al. 1997; Tanaka et al. 1994). On the other hand, MSTl receptive field size increases with eccentricity and at 10° eccentricity the receptive field width is about 10° (Eifuku and Wurtz 1998; Tanaka et al. 1994). This is relatively close to MT receptive field size. The pRF width of TO-2 at 10° eccentricity is 20–25°, which is again larger than RF estimates of MSTl, but the relatively small difference in pRF sizes between TO-1 and TO-2 supports the idea that TO-2 corresponds to MSTl rather than to MSTd.

In monkey the response to ipsilateral stimuli differs between MT and MSTd. MT neurons respond no further than 10–15° into the ipsilateral field (Desimone and Ungerleider 1986). By contrast, neurons in MSTd responded to stimuli as far as 30–40° into the ipsilateral field (Raiguel et al. 1997). Ipsilateral responses of MSTl neurons are not reported as far as we know. The responses in TO-2 extend further into the ipsilateral field than the responses in TO-1, but the difference in visual field coverage is much smaller than that between MT and MSTd, again supporting the correspondence between TO-2 and MSTl. On the other hand, if we assume TO-2 corresponds to MSTl, we would expect a human homologue of MSTd—a corresponding region just outside TO-2—to respond more strongly to the ipsilateral motion localizer. We did not find evidence for such an "MSTd" region in most hemispheres (Supplemental Figs. S4 and S8). This might be explained by our relatively small stimulus (10° in radius) that may elicit only weak responses from the huge RF sizes proposed to exist in MSTd. It is also possible that the dorsal part of TO-2 might overlap with MSTd for some subjects.

The larger pRF size measured with fMRI than the neuronal RF size measured with monkey electrophysiology has many possible explanations. The pRF size estimate depends on the mean size of the neuronal receptive field size as well as the scatter of neuronal RF center locations within the voxel. Simulations indicate that the contribution of the position variance for these maps is relatively small (Supplemental Fig. S16) and thus we think position variance is unlikely to explain the difference. On the other hand, it is likely that the sampling biases of electrodes and BOLD signals differ. Thus the receptive field sizes estimated with these two methods may reflect differences in the sampled populations. Another explanation is that the pRF size may include both the classical neuronal RF and extraclassical RF, perhaps creating the larger size. It is also important to emphasize how different the stimuli and measurement conditions are and to remember that estimates of receptive field size can depend significantly on aspects of the stimulus. In the human experiments we used large contrast patterns, whereas electrophysiological recordings generally use small isolated targets—this difference could result in different size estimation. The difference might also be due to species differences.

Visual field map organization

A model of the map organization on the lateral occipital surface is shown in Fig. 9. In this model the TO maps form part of a sequence of maps that extends along the lateral occipital lobe. This model differs from previous observations in several ways. First, other studies have failed to demonstrate retinotopy in these regions (Hansen et al. 2007; Tootell and Hadjikhani 2001); indeed many authors have referred to this part of cortex as nonretinotopic (Grill-Spector et al. 1998; Tyler et al. 2005).

Second, we demonstrate contiguous maps, where others questioned contiguity. Larsson and Heeger (2006) reported that LO-2 directly abutted MT+ for some hemispheres, whereas the two areas were separated by a short distance in other hemispheres. We support their suggestion that this separation may be an artifact of the conventional MT+ localizer.

It should be noted that the model for retinotopic maps used here may be incorrect and one could test for other models. For example, there may be one or two more hemifield representations that share the foveal representation with TO-1 and TO-2. In this case, angle representation might change along a circle for these visual fields as in the V1–V3 cluster (Wandell et al. 2005).

A further question concerns the organization of the region anterior to V3. Hansen et al. (2007) argue that adjacent and anterior to V3d there is a representation of a portion of the lower vertical meridian, but they assert that this representation is part of the V4 visual field map (V4d), not the LO-1 map. Here we follow Larsson and Heeger's convention, but further studies are necessary to clarify this issue.

Using new experimental and computational methods, we are able to reliably partition MT+ into two distinct visual field maps in the temporal occipital cortex. The response properties of these TO maps match the proposed functional dissociation of MT and MST (Dukelow et al. 2001; Huk et al. 2002). The ability to identify these maps securely should permit many more detailed analyses of the specific functional responses within these maps. The identification of the TO maps will allow more detailed exploration of the response properties of human motion-sensitive cortex and potential homologies to monkey visual areas.

REFERENCES

Allman JM, Kaas JH. A representation of the visual field in the caudal third of the middle temporal gyrus of the owl monkey (*Aotus trivirgatus*). *Brain Res* 31: 85–105, 1971.

Ashburner J, Friston K. Rigid body registration. In: *Human Brain Function* (2nd ed.), edited by Frackowiak RSJ, Friston KJ, Frith C, Dolan R, Friston KJ, Price CJ, Zeki S, Ashburner J, Penny WD. San Diego, CA: Academic Press/Elsevier Science, 2003, p. 635–654.

Bandettini PA, Jesmanowicz A, Wong EC, Hyde JS. Processing strategies for time-course data sets in functional MRI of the human brain. *Magn Reson Med* 30: 161–173, 1993.

Boussaoud D, Ungerleider LG, Desimone R. Pathways for motion analysis: cortical connections of the medial superior temporal and fundus of the superior temporal visual areas in the macaque. *J Comp Neurol* 296: 462–495, 1990.

Boynton GM, Engel SA, Glover GH, Heeger DJ. Linear systems analysis of functional magnetic resonance imaging in human V1. *J Neurosci* 16: 4207–4221, 1996.

Brainard DH. The Psychophysics Toolbox. *Spat Vis* 10: 433–436, 1997.

Brewer AA, Press WA, Logothetis NK, Wandell BA. Visual areas in macaque cortex measured using functional magnetic resonance imaging. *J Neurosci* 22: 10416–10426, 2002.

Britten KH, Newsome WT, Shadlen MN, Celebrini S, Movshon JA. A relationship between behavioral choice and the visual responses of neurons in macaque MT. *Vis Neurosci* 13: 87–100, 1996.

Britten KH, Shadlen MN, Newsome WT, Movshon JA. The analysis of visual motion: a comparison of neuronal and psychophysical performance. *J Neurosci* 12: 4745–4765, 1992.

Cavanaugh JR, Bair W, Movshon JA. Selectivity and spatial distribution of signals from the receptive field surround in macaque V1 neurons. *J Neurophysiol* 88: 2547–2556, 2002.

Desimone R, Ungerleider LG. Multiple visual areas in the caudal superior temporal sulcus of the macaque. *J Comp Neurol* 248: 164–189, 1986.

DeYoe EA, Carman GJ, Bandettini P, Glickman S, Wieser J, Cox R, Miller D, Neitz J. Mapping striate and extrastriate visual areas in human cerebral cortex. *Proc Natl Acad Sci USA* 93: 2382–2386, 1996.

Dougherty RF, Koch VM, Brewer AA, Fischer B, Modersitzki J, Wandell BA. Visual field representations and locations of visual areas V1/2/3 in human visual cortex. *J Vis* 3: 586–598, 2003.

Duffy CJ, Wurtz RH. Sensitivity of MST neurons to optic flow stimuli. II. Mechanisms of response selectivity revealed by small-field stimuli. *J Neurophysiol* 65: 1346–1359, 1991.

Dukelow SP, DeSouza JFX, Culham JC, van den Berg AV, Menon RS, Vilis T. Distinguishing subregions of the human MT plus complex using visual fields and pursuit eye movements. *J Neurophysiol* 86: 1991–2000, 2001.

Dumoulin SO, Bittar RG, Kabani NJ, Baker CL Jr, Le Goualher G, Bruce Pike G, Evans AC. A new anatomical landmark for reliable identification of human area V5/MT: a quantitative analysis of sulcal patterning. *Cereb Cortex* 10: 454–463, 2000.

Dumoulin SO, Wandell BA. Population receptive field estimates in human visual cortex. *Neuroimage* 39: 647–660, 2008.

Duncan RO, Boynton GM. Cortical magnification within human primary visual cortex correlates with acuity thresholds. *Neuron* 38: 659–671, 2003.

Eifuku S, Wurtz RH. Response to motion in extrastriate area MSTl: center–surround interactions. *J Neurophysiol* 80: 282–296, 1998.

Eifuku S, Wurtz RH. Response to motion in extrastriate area MSTl: disparity sensitivity. *J Neurophysiol* 82: 2462–2475, 1999.

Engel SA, Glover GH, Wandell BA. Retinotopic organization in human visual cortex and the spatial precision of functional MRI. *Cereb Cortex* 7: 181–192, 1997.

Felleman DJ, Kaas JH. Receptive-field properties of neurons in middle temporal visual area (MT) of owl monkeys. *J Neurophysiol* 52: 488–513, 1984.

Fize D, Vanduffel W, Nelissen K, Denys K, Chef d'Hotel C, Faugeras O, Orban GA. The retinotopic organization of primate dorsal V4 and surrounding areas: a functional magnetic resonance imaging study in awake monkeys. *J Neurosci* 23: 7395–7406, 2003.

Friston KJ, Fletcher P, Josephs O, Holmes A, Rugg MD, Turner R. Event-related fMRI: characterizing differential responses. *Neuroimage* 7: 30–40, 1998.

Glover GH. Deconvolution of impulse response in event-related BOLD fMRI. *Neuroimage* 9: 416–429, 1999a.

Glover GH. Simple analytic spiral K-space algorithm. *Magn Reson Med* 42: 412–415, 1999b.

Glover GH, Lai S. Self-navigated spiral fMRI: interleaved versus single-shot. *Magn Reson Med* 39: 361–368, 1998.

Grill-Spector K, Kushnir T, Hendler T, Edelman S, Itzchak Y, Malach R. A sequence of object-processing stages revealed by fMRI in the human occipital lobe. *Hum Brain Mapp* 6: 316–328, 1998.

Grill-Spector K, Malach R. The human visual cortex. *Annu Rev Neurosci* 27: 649–677, 2004.

Grill-Spector K, Sayres R, Ress D. High-resolution imaging reveals highly selective nonface clusters in the fusiform face area. *Nat Neurosci* 9: 1177–1185, 2006.

Hansen KA, Kay KN, Gallant JL. Topographic organization in and near human visual area V4. *J Neurosci* 27: 11896–11911, 2007.

Heyder J. *Optimierungsansatz zur simultanen Registrierung von fMRT-Bildern mit Volumenerhaltung* (MS thesis). Lübeck, Germany: Institute of Mathematics, Univ. of Lübeck, 2006.

Huk AC, Dougherty RF, Heeger DJ. Retinotopy and functional subdivision of human areas MT and MST. *J Neurosci* 22: 7195–7205, 2002.

Huk AC, Heeger DJ. Pattern-motion responses in human visual cortex. *Nat Neurosci* 5: 72–75, 2002.

Huk AC, Ress D, Heeger DJ. Neuronal basis of the motion aftereffect reconsidered. *Neuron* 32: 161–172, 2001.

Jancke D, Erlhagen W, Schoner G, Dinse HR. Shorter latencies for motion trajectories than for flashes in population responses of cat primary visual cortex. *J Physiol* 556: 971–982, 2004.

Komatsu H, Wurtz RH. Relation of cortical areas MT and MST to pursuit eye movements. I. Localization and visual properties of neurons. *J Neurophysiol* 60: 580–603, 1988.

Larsson J, Heeger DJ. Two retinotopic visual areas in human lateral occipital cortex. *J Neurosci* 26: 13128–13142, 2006.

Maes F, Collignon A, Vandermeulen D, Marchal G, Suetens P. Multimodality image registration by maximization of mutual information. *IEEE Trans Med Imaging* 16: 187–198, 1997.

Malach R, Reppas JB, Benson RR, Kwong KK, Jiang H, Kennedy WA, Ledden PJ, Brady TJ, Rosen BR, Tootell RB. Object-related activity revealed by functional magnetic resonance imaging in human occipital cortex. *Proc Natl Acad Sci USA* 92: 8135–8139, 1995.

Maunsell JH, Van Essen DC. Functional properties of neurons in middle temporal visual area of the macaque monkey. I. Selectivity for stimulus direction, speed, and orientation. *J Neurophysiol* 49: 1127–1147, 1983.

Maunsell JH, Van Essen DC. Topographic organization of the middle temporal visual area in the macaque monkey: representational biases and the relationship to callosal connections and myeloarchitectonic boundaries. *J Comp Neurol* 266: 535–555, 1987.

Morrone MC, Tosetti M, Montanaro D, Fiorentini A, Cioni G, Burr DC. A cortical area that responds specifically to optic flow, revealed by fMRI. *Nat Neurosci* 3: 1322–1328, 2000.

Orban GA, Van Essen D, Vanduffel W. Comparative mapping of higher visual areas in monkeys and humans. *Trends Cogn Sci* 8: 315–324, 2004.

Pelli DG. The VideoToolbox software for visual psychophysics: transforming numbers into movies. *Spat Vis* 10: 437–442, 1997.

Raiguel S, Van Hulle MM, Xiao DK, Marcar VL, Lagae L, Orban GA. Size and shape of receptive fields in the medial superior temporal area (MST) of the macaque. *Neuroreport* 8: 2803–2808, 1997.

Rees G, Friston K, Koch C. A direct quantitative relationship between the functional properties of human and macaque V5. *Nat Neurosci* 3: 716–723, 2000.

Rolls ET, Aggelopoulos NC, Zheng F. The receptive fields of inferior temporal cortex neurons in natural scenes. *J Neurosci* 23: 339–348, 2003.

Salzman CD, Murasugi CM, Britten KH, Newsome WT. Microstimulation in visual area MT: effects on direction discrimination performance. *J Neurosci* 12: 2331–2355, 1992.

Saygin AP, Sereno MI. Retinotopy and attention in human occipital, temporal, parietal, and frontal cortex. *Cereb Cortex* 18: 2158–2168, 2008.

Sereno SC. Resolution of lexical ambiguity: evidence from an eye movement priming paradigm. *J Exp Psychol Learn Mem Cogn* 21: 582–595, 1995.

Solomon SG, Peirce JW, Lennie P. The impact of suppressive surrounds on chromatic properties of cortical neurons. *J Neurosci* 24: 148–160, 2004.

Tanaka K, Sugita Y, Moriya M, Saito H. Analysis of object motion in the ventral part of the medial superior temporal area of the macaque visual cortex. *J Neurophysiol* 69: 128–142, 1993.

Teo PC, Sapiro G, Wandell BA. Creating connected representations of cortical gray matter for functional MRI visualization. *IEEE Trans Med Imaging* 16: 852–863, 1997.

Tootell RB, Hadjikhani N. Where is "dorsal V4" in human visual cortex? Retinotopic, topographic and functional evidence. *Cereb Cortex* 11: 298–311, 2001.

Tootell RB, Reppas JB, Kwong KK, Malach R, Born RT, Brady TJ, Rosen BR, Belliveau JW. Functional analysis of human MT and related visual cortical areas using magnetic resonance imaging. *J Neurosci* 15: 3215–3230, 1995.

Tootell RB, Taylor JB. Anatomical evidence for MT and additional cortical visual areas in humans. *Cereb Cortex* 5: 39–55, 1995.

Tyler CW, Baseler HA, Kontsevich LL, Likova LT, Wade AR, Wandell BA. Predominantly extra-retinotopic cortical response to pattern symmetry. *Neuroimage* 24: 306–314, 2005.

Tyler CW, Wade AR. Extended concepts of occipital retinotopy. *Curr Med Imaging Rev* 1: 319–329, 2005.

Ungerleider LG, Desimone R. Cortical connections of visual area MT in the macaque. *J Comp Neurol* 248: 190–222, 1986.

Vanduffel W, Fize D, Mandeville JB, Nelissen K, Van Hecke P, Rosen BR, Tootell RB, Orban GA. Visual motion processing investigated using contrast agent-enhanced fMRI in awake behaving monkeys. *Neuron* 32: 565–577, 2001.

Victor JD, Purpura K, Katz E, Mao B. Population encoding of spatial frequency, orientation, and color in macaque V1. *J Neurophysiol* 72: 2151–2166, 1994.

Walters NB, Egan GF, Kril JJ, Kean M, Waley P, Jenkinson M, Watson JD. In vivo identification of human cortical areas using high-resolution MRI: an approach to cerebral structure-function correlation. *Proc Natl Acad Sci USA* 100: 2981–2986, 2003.

Wandell BA, Brewer AA, Dougherty RF. Visual field map clusters in human cortex. *Philos Trans R Soc Lond B Biol Sci* 360: 693–707, 2005.

Wandell BA, Chial S, Backus BT. Visualization and measurement of the cortical surface. *J Cogn Neurosci* 12: 739–752, 2000.

Watson JD, Myers R, Frackowiak RS, Hajnal JV, Woods RP, Mazziotta JC, Shipp S, Zeki S. Area V5 of the human brain: evidence from a combined study using positron emission tomography and magnetic resonance imaging. *Cereb Cortex* 3: 79–94, 1993.

Worsley KJ, Liao CH, Aston J, Petre V, Duncan GH, Morales F, Evans AC. A general statistical analysis for fMRI data. *Neuroimage* 15: 1–15, 2002.

Zeki S, Watson JD, Lueck CJ, Friston KJ, Kennard C, Frackowiak RS. A direct demonstration of functional specialization in human visual cortex. *J Neurosci* 11: 641–649, 1991.